APL Photonics

Graphene/Ge microcrystal photodetectors with enhanced infrared responsivity

Cite as: APL Photonics **7**, 046106 (2022); https://doi.org/10.1063/5.0082421
Submitted: 15 December 2021 • Accepted: 22 March 2022 • Published Online: 13 April 2022

Virginia Falcone, **Andrea Ballabio**, **Andrea Barzaghi, et al.**

ARTICLES YOU MAY BE INTERESTED IN

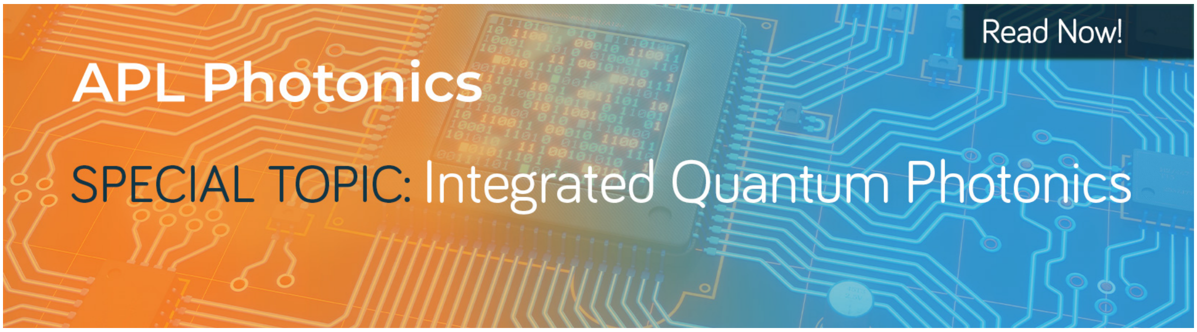

APL Photonics **7**, 046106 (2022); https://doi.org/10.1063/5.0082421

APL Photonics ARTICLE scitation.org/journal/app

Graphene/Ge microcrystal photodetectors with enhanced infrared responsivity

Cite as: APL Photon. 7, 046106 (2022); doi: 10.1063/5.0082421
Submitted: 15 December 2021 • Accepted: 22 March 2022 •
Published Online: 13 April 2022

Virginia Falcone,[1] Andrea Ballabio,[1,a)] Andrea Barzaghi,[1] Carlo Zucchetti,[1] Luca Anzi,[1] Federico Bottegoni,[1] Jacopo Frigerio,[1] Roman Sordan,[1] Paolo Biagioni,[2] and Giovanni Isella[1]

AFFILIATIONS

[1] L-NESS Dipartimento di Fisica, Politecnico di Milano, Via Anzani 42, I-22100 Como, Italy
[2] Dipartimento di Fisica, Politecnico di Milano, Piazza Leonardo da Vinci 32, I-20133 Milano, Italy

[a)] Author to whom correspondence should be addressed: andrea.ballabio@polimi.it

ABSTRACT

We report on the electrical and optical properties of microcrystal arrays obtained by depositing Ge on a deeply patterned Si substrate. Finite difference time domain simulations indicate that the faceted morphology and high refractive index of Ge microcrystals lead to strong light trapping effects, enhancing infrared light absorption in the spectral window between the direct and indirect absorption edge of Ge (≈1550–1800 nm). This is experimentally confirmed by fabricating microcrystal-based Ge-on-Si photodiodes employing graphene as a top transparent contact. In these devices, the ratio between the responsivities at 1550 and 1700 nm is more than ten times larger than that of photodiodes based on conventional Ge-on-Si epilayers.

INTRODUCTION

The epitaxial growth of germanium on silicon[1] has fostered the development of near infrared detectors for telecom[2] and imaging[3] applications, and at the present time, their fabrication is fully compatible with 300 mm CMOS foundries.[4] The long wavelength (λ) responsivity of these devices is limited to ~1550 nm, corresponding to the direct energy gap of Ge, $E_g{}^{\Gamma} = 0.8$ eV. Indeed, the absorption coefficient at the indirect gap $E_g{}^{L} = 0.66$ eV ($\lambda \approx 1800$ nm) is roughly two orders of magnitudes smaller than that above the direct gap threshold.[5] A sizable absorption within the 1550–1800 nm window would, therefore, require exceedingly thick epilayers, resulting in wafer bowing[6] and crack formation.[7] As a result, the typical responsivity of vertically illuminated photodiodes based on Ge-on-Si epilayers falls in the 0.3–0.7 A/W range at 1550 nm but drops in the mA/W range at 1700 nm.[2] Yet, an extended infrared absorption would be beneficial for imaging applications since long wavelength radiation is less affected by Rayleigh and Mie scattering, which limits visibility in fog and dusty conditions.[8]

A viable route to enhance the responsivity of Ge-on-Si photodetectors in the 1550–1800 nm region might be to exploit the micro-structuring of the absorbing layer to increase the effective volume of interaction between light and matter.[9,10] Within this frame, the *top-down* etching of Ge wafers[11] or Ge-on-Si epilayers[12] has led to the fabrication of nanowire arrays behaving as p–i–n photodetectors with a tunable responsivity resulting from the combined effect of nanowire's photonic resonances and the applied bias. The nano-structuring allowed for the tuning of the responsivity within the 400–1600 nm window without any sizable effect on photoresponse in the indirect gap region.[12,13] A *bottom-up* approach, based on substrate patterning and selective Ge heteroepitaxy, has resulted in the formation of nanodots,[14] which can also be used for photodetection,[15] however, with an extremely poor active volume, not suitable for imaging applications.

Substrate patterning at the micrometer scale, combined with out-of-equilibrium deposition of Ge, results in the formation of several micrometer tall Ge microcrystals.[16] The fundamental physical phenomena leading to the formation of microcrystals have been clarified by means of two-dimensional kinetic models[17] and three-dimensional (3D) phase-field models.[18] Notably, the crystal facet evolution during growth leads to the expulsion of threading dislocations[19] and, as a consequence, to the increase of recombination lifetimes.[20] Moreover, the regular surface texturing and volume tessellation, featured by micro-crystal arrays, give rise to light trapping effects, which have previously been experimentally observed in silicon microcrystals.[21]

Here, we propose the use of micrometer-sized Ge crystals epitaxially grown on a deeply patterned Si substrate[16] as the building block for Ge-on-Si photodetectors with extended infrared responsivity. First, we demonstrate, by means of finite-difference time-domain (FDTD) modeling, that light absorption in Ge-on-Si microcrystals in the 1550–1700 nm window is increased by a factor of ~2.5, as compared to a flat epilayer.[21] Then, we exploit such unique optical properties to fabricate p–i–n photodetectors with a graphene top contact to connect microcrystal arrays in parallel. The photoresponse of microcrystal-based detectors, within the 1550–1700 nm region, outperforms that of a reference planar device by up to one order of magnitude.

Ge MICROCRYSTAL GROWTH AND FDTD MODELING

To foster nucleation of microcrystals, vertical pillars were etched in a Si wafer by means of optical lithography and reactive-ion etching. The width (W) of the Si square-shaped pillars and the periodicity of the pattern ($W + G$, where G is the gap between Si pillars) between the adjacent pillars were in the micrometer range. The dimensions of three different patterns, A, B and C, used in the fabrication of photodiodes, are reported in Table I.

Ge-on-Si microcrystals were grown by low-energy plasma-enhanced chemical vapor deposition (LEPECVD),[22] a variant of CVD used to obtain the high deposition rate (≈4 nm/s) and the out-of-equilibrium conditions required for the formation of microcrystals.[18,19] A p–i–n heterojunction was realized by depositing 5 μm of nominally intrinsic Ge followed by 200 nm of p-type (boron concentration $\approx 5 \times 10^{18}$ cm^{-3}) Ge on the heavily n-type patterned Si substrate (arsenic concentration $\approx 1 \times 10^{19}$ cm^{-3}). Figure 1 shows the top [(a)–(c)] and cross-sectional [(d)–(f)] view scanning electron microscopy (SEM) images of the microcrystal arrays obtained from patterns A, B, and C. The SEM images were used to extract the microcrystal morphology required for the FDTD calculations implemented within the commercial software Ansys Lumerical FDTD.[23] This procedure was repeated for each of the three patterns under investigation, thus considering the different facets' extension, inclination, and pillar gaps featured by the microcrystals. The simulation domain comprises a single microcrystal, as shown in Fig. 2. Periodic boundary conditions were applied at the correct distance for each pattern to take the periodicity of the microcrystal array into account.

TABLE I. Dimensions of the square-shaped Si pillars of three patterns used in the fabrication of photodiodes. W is the pillar width, and W + G is the periodicity of the patterns. In all cases, the etched depth was 8 μm.

Pattern	W (μm)	W + G (μm)
A	2	4
B	2	6
C	4	7

In the FDTD calculations, the microcrystals were vertically illuminated by a plane wave in the 1300–1700 nm range. Two monitors, represented by the green lines above and below the microcrystal array in Fig. 2(a), yield the difference $1 - R$ between the incoming and the reflected power (top monitor) and the fraction T of the transmitted power (bottom monitor). The difference between the top and bottom monitors yields the fraction of absorbed power $A = 1 - R - T$. The spatial distribution of the absorbed power density at $\lambda = 1400$ nm, shown in Fig. 2(b), highlights the role played by the microcrystal faceting in trapping the incoming radiation. In the FDTD simulations, wavelength dependent "hotspot" patterns

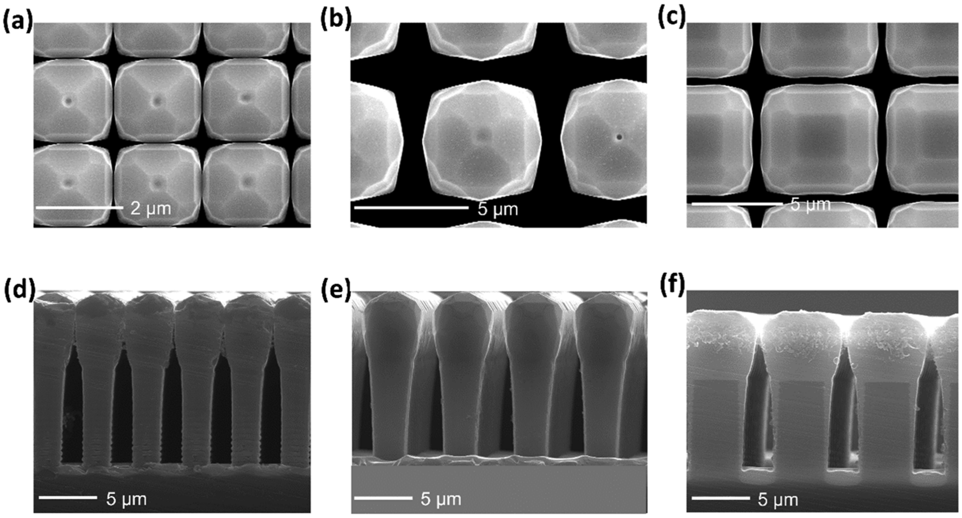

FIG. 1. Epitaxially grown microcrystals on a patterned Si substrate. (a)–(c) SEM images (top view) of microcrystals A, B, and C. (d)–(f) SEM images of the cross section of microcrystals A, B, and C. In (f), the microcrystals were diced approximately through their central part, making the buried Si pillar visible.

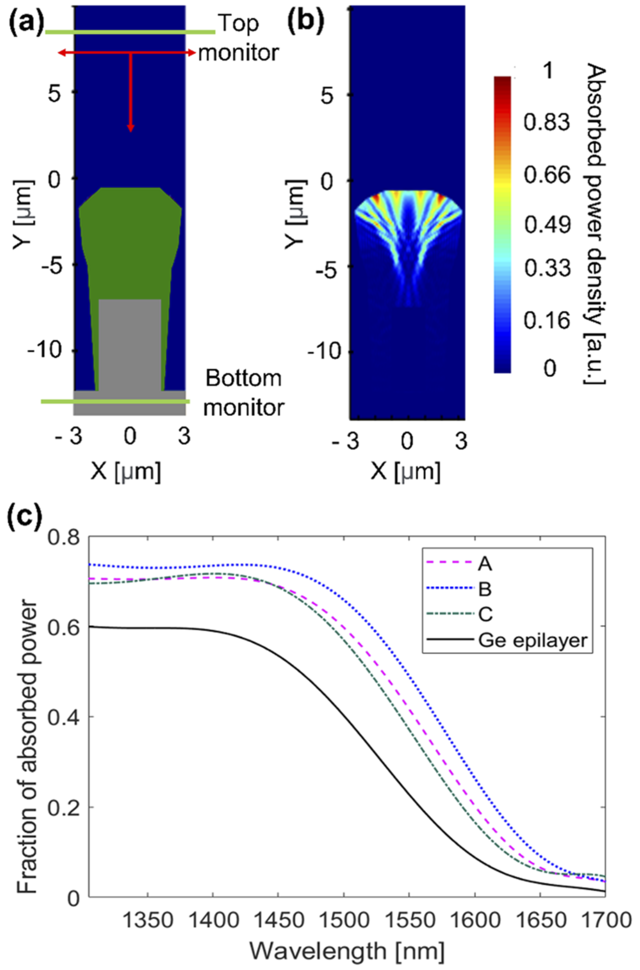

FIG. 2. Simulation of absorption in the fabricated microcrystals. (a) Schematic of the simulation area. (b) Absorbed power density map at $\lambda = 1400$ nm . (c) Fraction of absorbed power obtained from the fitting with a seventh-order polynomial function for patterns A (magenta dashed line), B (blue dotted line), and C (green dashed-dotted line) and for a continuous Ge film (black solid line) featuring the same thickness of the microcrystals.

are clearly visible, yet we expect their exact spectral position to be strongly dependent on the geometrically perfect morphology of the polyhedral used to reconstruct the microcrystals.

Figure 2(c) shows the fraction of the absorbed power A for the three patterns under investigation, together with the reference case of a planar Ge epilayer. The power fraction absorbed by the microcrystals was smoothed using a polynomial interpolation (see the supplementary material) to remove sharp spectral features caused by the geometrically perfect shapes used for modeling. These artifacts are absent in experimental data because of broadening effects[21] induced by deviations from the ideal shape and inhomogeneities within the microcrystal array.

For the three patterns, the absorbed power exceeds that of the equivalent epilayer, especially in the indirect transition wavelength range. Around 1700 nm, the absorbed power of the patterns is about 2.5 times larger than the one of a flat Ge layer. Indeed, within the spectral window between the direct and indirect gap of Ge, infrared light undergoes a more intense internal reflection and trapping, as compared to shorter wavelengths, which are strongly absorbed by the microcrystals. This results in a strong absorption enhancement in the 1550–1700 nm region.

FABRICATION OF GRAPHENE/Ge MICROCRYSTAL PHOTODETECTORS

To experimentally verify the enhanced absorption in Ge-on-Si microcrystals, vertically illuminated photodiodes were fabricated. The main challenge in the fabrication of photodiodes based on Ge-on-Si microcrystals is the formation of a top transparent contact that can adapt to the 3D morphology of the microcrystals and bridge the 100–200 nm gap between adjacent microcrystals. Graphene was used as a suspended continuous top contact featuring an extremely high transparency (>97% for a monolayer)[24] obtaining the device schematically shown in Fig. 3(a).

As a first fabrication step, a 100 nm-thick SiO_2 layer was deposited by plasma-enhanced CVD on both the patterned and unpatterned area of the Si substrate. Then, by optical lithography and HF wet etching, the SiO_2 layer was removed from the patterned areas, which were ~100 × 100 μm^2 in size. An oxide window of the identical dimensions was formed in the unpatterned region with the purpose of fabricating a reference photodiode based on a conventional Ge-on-Si epilayer. Ti/Au (5/150 nm) metal pads, acting as top ohmic contacts, were deposited by *e*-beam evaporation on the SiO_2 layer close to the oxide windows, as shown in Fig. 3(b). The bottom contact was evaporated on the backside of the Si wafer.

The electrical connection between the Ge microcrystals and the top metal pad was first attempted by wet transfer[25] of a graphene monolayer grown by CVD on a Cu foil.[26] The wet transfer process, however, led to the discontinuities in the graphene monolayer, with several cuts forming during the drying phase. This is probably due to capillary forces present in the 100–200 nm gaps separating adjacent microcrystals.[27] This issue was overcome by performing the wet transfer process twice, with a single drying step after the second transfer. The two layers of graphene were found to be strong enough to withstand capillary forces, resulting in the continuous conductive layer shown in Fig. 3(c) featuring a transparency of ~95%.[24]

At variance with most graphene/semiconductor photodetectors reported in the literature,[28] where the depletion region is defined by the Schottky barrier at the graphene/semiconductor junction, a built-in potential is already formed within the microcrystal by the p–i–n doping profile (see the supplementary material). It is well known that Ge surface states pin the Fermi level very close to the valence band, favoring the formation of an ohmic contact at the graphene/Ge interface.[29] The I–V curve of one of the fabricated devices is shown in Fig. 3(d). A dark current density of ≈2 mA/cm^2 is obtained at a bias of −1 V, in agreement with the values reported for conventional Ge-on-Si photodiodes.[2]

PHOTORESPONSE OF GRAPHENE/Ge MICROCRYSTALS

The optical characterization of the graphene/Ge-on-Si microcrystal photodetectors was performed in the wavelength range

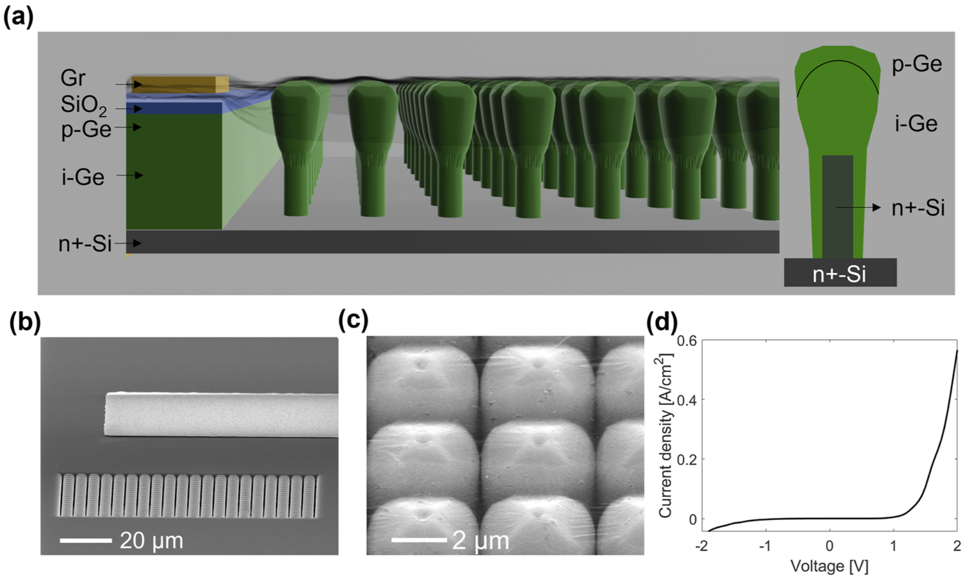

FIG. 3. Microcrystals with a top graphene contact. (a) Schematic of the fabricated device (left) and the doping profile (right) of a single microcrystal. (b) SEM image of the Ti/Au metal pad deposited on the SiO_2 layer close to the patterned area. (c) SEM image of the Ge microcrystals connected by two layers of graphene. The contact point between the graphene layers and the microcrystal top is clearly visible. (d) Current density of pattern A as a function of voltage.

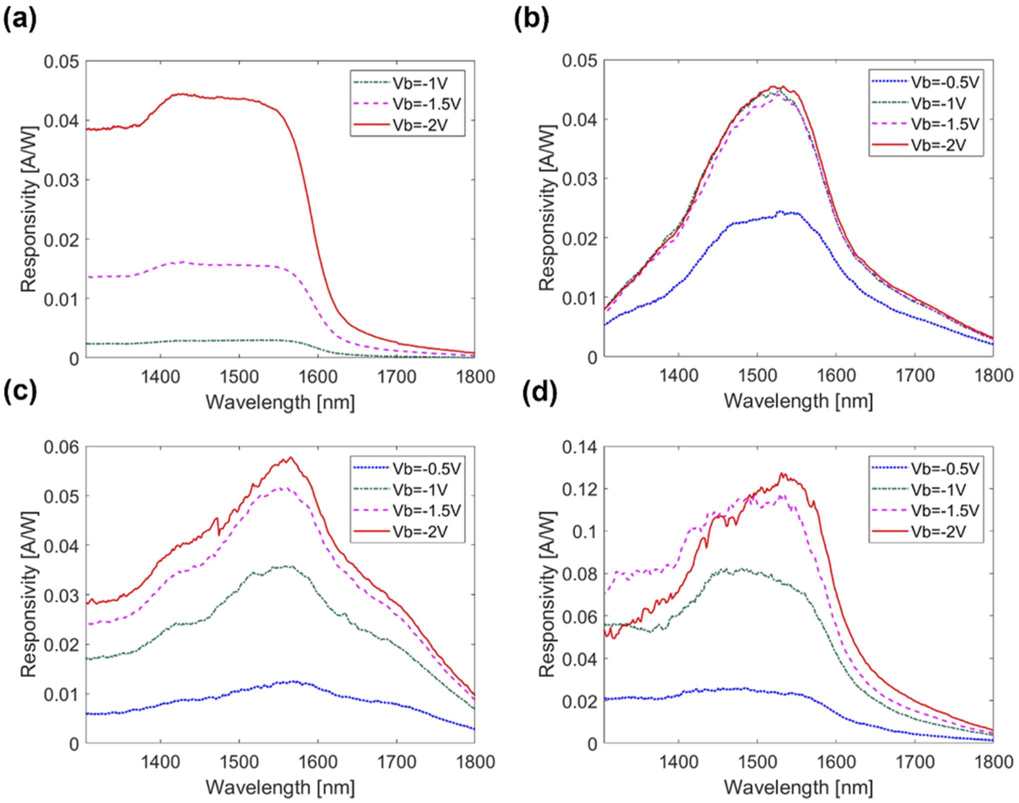

FIG. 4. Responsivity of the fabricated photodiodes. (a) Responsivity of the graphene/Ge epilayer device under reverse bias. (b)–(d) Responsivity of the graphene/Ge microcrystal device under reverse bias (patterns A, B, and C, respectively).

between 1300 and 1800 nm, exploiting the monochromatized light of a supercontinuum laser (SuperK Extreme EXW-12, NKT Photonics) with half-width at half-maximum about 10 meV. Light was focused on the sample surface by an objective, yielding a spot size smaller than the patterned area, with a power density almost uniform within the spot. The light beam was chopped at 831 Hz, and the photocurrent was acquired by demodulating the current measured between the top graphene contact and a bottom electrode with a lock-in amplifier. Figure 4(a) shows the responsivity of the planar device under reverse bias between −2 and 0 V. The non-negligible background doping of the 5 μm-thick p-type Ge layer, estimated to be ~1×10^{16} cm^{-3}, results in the formation of a space charge region substantially shorter than the i-layer. By increasing the reverse bias, the depletion region and, therefore, the charge collection efficiency increase, leading to a substantial enhancement of the responsivity. A similar behavior is also observed in the case of the graphene/Ge-on-Si microcrystal devices whose responsivity is reported in Figs. 4(b)–4(d). We note that the peak responsivity is higher in microcrystal-based devices, confirming the increase in the fraction of absorbed power predicted by the FDTD modeling. This could also be due to the lower density of threading dislocations within the microcrystals, as compared to conventional epilayers, or to the 3D nature of the p–i–n junctions, which might affect the photocarrier collection efficiency.[21]

The spectral shape of the responsivity is strongly affected by the microcrystal morphology, and a strong enhancement of the long wavelength ($\lambda > 1550$ nm) response is observed for the three investigated patterns. Figure 5(a) shows the ratio between the microcrystal and planar epilayer absorbance, as obtained by the FDTD simulations [see Fig. 2(c)]. The ratio between the experimental responsivities of the microcrystal- and planar-based photodiodes is reported in Fig. 5(b). The responsivity ratio of the three patterns confirms the trend observed in the absorbed power simulations: a clear increase in absorbance and responsivity is seen in the wavelength range between the direct and indirect gap of Ge.

Given the good qualitative agreement between absorbance and responsivity, a quantitative estimation of the enhanced long wavelength photo-response can be obtained by calculating the ratio of the responsivity of the microcrystals and reference photodiodes at a fixed reverse bias of −2 V. At 1700 nm, this ratio is 4 for pattern A, 10 for pattern B, and 7 for pattern C. Such responsivity enhancement exceeds the increased absorption expected from the FDTD simulations.

Within a simple one-dimensional model, the responsivity[30] of a p–i–n photodiode can be expressed as $R \propto \eta(1 - e^{-\alpha d})$, where η is the collection efficiency, α is the absorption coefficient, and d is the thickness of the absorption layer. In microcrystals, besides the already mentioned reduced density of threading dislocation, the 3D nature of the p–i–n doping profile leads to an electric field distribution substantially different from that of a planar photodiode. These effects might have a strong impact on η, enhancing the responsivity beyond what could be expected from the enhanced absorption alone.

The time response of the graphene/Ge-on-Si microcrystal device was evaluated (see the supplementary material) by considering the contributions of drift current, diffusion current, and RC time constant to the 3 dB cut-off frequency. Due to the non-negligible residual doping and relatively high dielectric constant of Ge, the 5 μm-tall microcrystals are to a large extent quasi-neutral. The dominating transport mechanism is, therefore, diffusion, which limits the 3 dB cut-off frequency to ≈150 MHz. Although this value would be unacceptable for telecom applications, it is still suitable for imaging and sensing applications, which motivated our work.

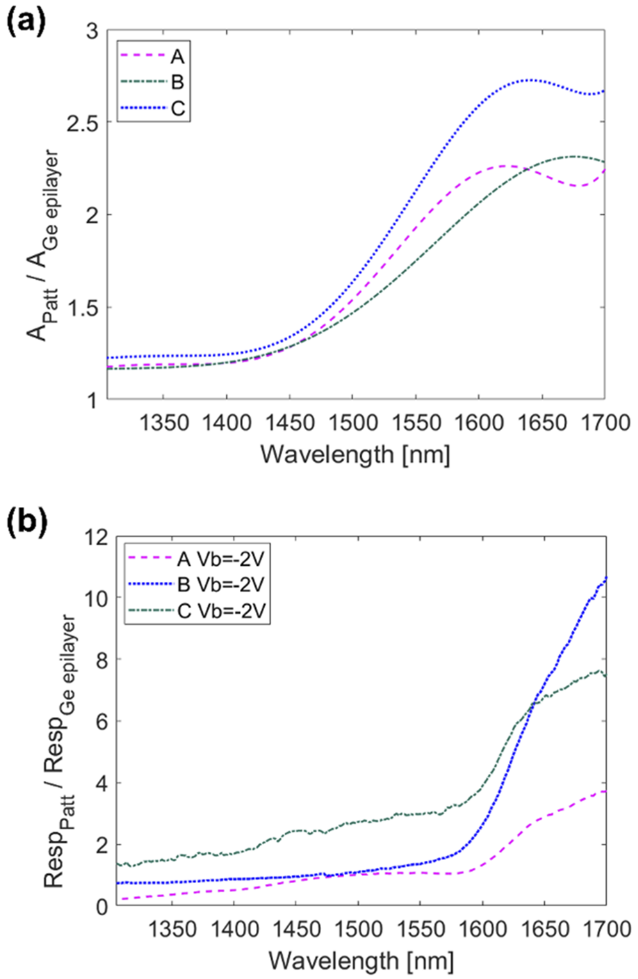

FIG. 5. Comparison between the optical properties of the patterned and continuous Ge films. (a) Ratio of the fraction of the absorbed power of the patterned and continuous Ge films. (b) Responsivity ratio between the patterned and continuous Ge films.

CONCLUSIONS

The optical properties of 3D Ge-on-Si microcrystals were analyzed by the FDTD simulations, demonstrating an enhancement of the absorbed power, as compared to a planar Ge epilayer, especially in the wavelength region between the direct and the indirect gap of Ge. This feature can be ascribed to multiple internal reflections, induced by microcrystal faceting, which increase the optical path in the 1550–1700 nm range. Microcrystal-based photodetectors were fabricated by suspending two graphene layers on microcrystal arrays, thus obtaining a transparent top contact. Responsivity measurements demonstrated that the photoresponse was strongly influenced by the microcrystal morphology, and a photoresponse enhancement in the 1550–1700 nm window was observed in agreement with the FDTD modeling. The ratio of the photoresponse at 1700 and 1550 nm ranges between 12% and 56% for the three patterns analyzed in this work, which should be compared with a value of ≈2% typically observed in conventional Ge-on-Si photodiodes.[1] This makes the fabricated devices suitable for imaging and sensing applications in the technologically relevant 1300–1700 nm range.

SUPPLEMENTARY MATERIAL

See the supplementary material for details about the fraction of the light absorbed by Ge microcrystals as obtained by FDTD calculations.

ACKNOWLEDGMENTS

This work was funded by the EU Horizon's 2020 projects microSPIRE under Grant No. 766955 and Graphene Flagship Core 3 under Grant No. 881603. The authors would like to thank F. Mancarella for the microfabrication of patterned substrates and Polifab for the access to the facility for the device fabrication.

AUTHOR DECLARATIONS

Conflict of Interest

The authors have no conflicts to disclose.

DATA AVAILABILITY

The data that support the findings of this study are available from the corresponding author upon reasonable request.

REFERENCES

[1] L. Colace, G. Masini, G. Assanto, H.-C. Luan, K. Wada, and L. C. Kimerling, Appl. Phys. Lett. **76**, 1231 (2000).

[2] J. Michel, J. Liu, and L. C. Kimerling, Nat. Photonics **4**, 527 (2010).

[3] R. Kaufmann, G. Isella, A. Sanchez-Amores, S. Neukom, A. Neels, L. Neumann, A. Brenzikofer, A. Dommann, C. Urban, and H. von Känel, J. Appl. Phys. **110**, 023107 (2011).

[4] D. Marris-Morini, L. Virot, C. Baudot, J.-M. Fédéli, G. Rasigade, D. Perez-Galacho, J.-M. Hartmann, S. Olivier, P. Brindel, P. Crozat, F. Bœuf, and L. Vivien, Opt. Express **22**, 6674 (2014).

[5] W. C. Dash and R. Newman, Phys. Rev. **99**, 1151 (1955).

[6] G. Capellini, M. De Seta, P. Zaumseil, G. Kozlowski, and T. Schroeder, J. Appl. Phys. **111**, 073518 (2012).

[7] D. Colombo, E. Grilli, M. Guzzi, S. Sanguinetti, S. Marchionna, and M. Bonfanti, J. Appl. Phys. **101**, 103519 (2007).

[8] D. Deirmendjian, Appl. Opt. **3**, 187 (1964).

[9] A. Solanki and K. Crozier, Appl. Phys. Lett **105**, 191115 (2014).

[10] J. M. Lee, J. W. Choung, J. Yi, D. H. Lee, M. Samal, D. K. Yi, C.-H. Lee, G.-C. Yi, U. Paik, and J. A. Rogers, Nano Lett. **10**, 2783 (2010).

[11] A. Solanki, S. Li, H. Park, and K. B. Crozier, ACS Photonics **5**, 520 (2018).

[12] S. Q. Li, A. Solanki, J. Frigerio, D. Chrastina, G. Isella, C. Zheng, A. Ahnood, K. Ganesan, and K. B. Crozier, ACS Photonics **6**, 735 (2019).

[13] A. I. Yakimov, A. A. Bloshkin, V. V. Kirienko, A. V. Dvurechenskii, and D. E. Utkin, JETP Lett. **113**, 498 (2021).

[14] G. Niu, G. Capellini, G. Lupina, T. Niermann, M. Salvalaglio, A. Marzegalli, M. A. Schubert, P. Zaumseil, H.-M. Krause, O. Skibitzki, M. Lehmann, F. Montalenti, Y.-H. Xie, and T. Schroeder, ACS Appl. Mater. Interfaces **8**, 2017 (2016).

[15] A. I. Yakimov, V. V. Kirienko, A. A. Bloshkin, D. E. Utkin, and A. V. Dvurechenskii, Nanomaterials **11**, 2302 (2021).

[16] C. V. Falub, H. von Känel, F. Isa, R. Bergamaschini, A. Marzegalli, D. Chrastina, G. Isella, E. Müller, P. Niedermann, and L. Miglio, Science **335**, 1330 (2012).

[17] R. Bergamaschini, F. Isa, C. V. Falub, P. Niedermann, E. Müller, G. Isella, H. von Känel, and L. Miglio, Surf. Sci. Rep. **68**, 390 (2013).

[18] M. Albani, R. Bergamaschini, A. Barzaghi, M. Salvalaglio, J. Valente, D. J. Paul, A. Voigt, G. Isella, and F. Montalenti, Sci. Rep. **11**, 18825 (2021).

[19] A. Marzegalli, F. Isa, H. Groiss, E. Müller, C. V. Falub, A. G. Taboada, P. Niedermann, G. Isella, F. Schäffler, F. Montalenti, H. von Känel, and L. Miglio, Adv. Mater. **25**, 4408 (2013).

[20] F. Pezzoli, F. Isa, G. Isella, C. V. Falub, T. Kreiliger, M. Salvalaglio, R. Bergamaschini, E. Grilli, M. Guzzi, H. von Känel, and L. Miglio, Phys. Rev. Appl. **1**, 044005 (2014).

[21] J. Pedrini, P. Biagioni, A. Ballabio, A. Barzaghi, M. Bonzi, E. Bonera, G. Isella, and F. Pezzoli, Opt. Express **28**, 24981 (2020).

[22] C. Rosenblad, H. R. Deller, A. Dommann, T. Meyer, P. Schroeter, and H. von Känel, J. Vac. Sci. Technol. A **16**, 2785 (1998).

[23] Lumerical, Inc., Release 2020a: FDTD Solutions, Canada, 2018, https://www.lumerical.com/products/fdtd/; accessed 24 November 2021.

[24] R. R. Nair, P. Blake, A. N. Grigorenko, K. S. Novoselov, T. J. Booth, T. Stauber, N. M. R. Peres, and A. K. Geim, Science **320**, 1308 (2008).

[25] J. W. Suk, A. Kitt, C. W. Magnuson, Y. Hao, S. Ahmed, J. An, A. K. Swan, B. B. Goldberg, and R. S. Ruoff, ACS Nano **5**, 6916 (2011).

[26] X. Li, W. Cai, J. An, S. Kim, J. Nah, D. Yang, R. Piner, A. Velamakanni, I. Jung, E. Tutuc, S. K. Banerjee, L. Colombo, and R. S. Ruoff, Science **324**, 1312 (2009).

[27] F. Traversi, F. J. Gúzman-Vázquez, L. G. Rizzi, V. Russo, C. S. Casari, C. Gómez-Navarro, and R. Sordan, New J. Phys. **12**, 023034 (2010).

[28] A. Di Bartolomeo, Phys. Rep. **606**, 1 (2016).

[29] A. Dimoulas, P. Tsipas, A. Sotiropoulos, and E. K. Evangelou, Appl. Phys. Lett. **89**, 252110 (2006).

[30] W. W. Gärtner, Phys. Rev. **116**, 84 (1959).